Available online at website: https://journal.bcrec.id/index.php/bcrec

Bulletin of Chemical Reaction Engineering & Catalysis, 21 (3) 2026, 569-585

Original Research Article

Enhanced Acid Orange 7 Adsorption by a Novel Organophosphorus-Modified Bentonite: Performance and Mechanistic Insights

Nouria Mahrez[1], Fatima Zohra Belkacem[1], Amine Amar[1], Mounir Khelifa[2], Ali Çoruh[3], Fatima Boucif[1], Fatiha Bessaha[1], Kheira Marouf-Khelifa[1], Amine Khelifa[1]*

[1]*Laboratoire de Structure, Elaboration et Applications des Matériaux Moléculaires (SEA2M), Département de Génie des Procédés, Faculté des Sciences et de la Technologie, Université Abdelhamid Ibn Badis, Mostaganem, Algeria.*

[2]*Laboratoire de Structure, Elaboration et Applications des Matériaux Moléculaires (SEA2M), Département de Génie des Procédés, Faculté des Sciences et de la Technologie, Université Ahmed Zabana, Relizane, Algeria.*

[3]*Department of Physics, Sakarya University, 54147-Kampus, Sakarya, Turkey.*

Received: 21th February 2026; Revised: 31th March 2026; Accepted: 1st April 2026
Available online: 5th April 2026; Published regularly: October 2026

Abstract

Water contamination by Acid Orange 7 (AO7), a widely used anionic azo dye in the textile industry, represents a major environmental concern due to its persistence and potential to generate toxic aromatic amines. Herein, we report the synthesis of a novel organobentonite (BPA6) via intercalation of phenylphosphonic acid into bentonite, an organoclay previously unexplored for pollutant removal. XRD analysis revealed an expansion of the basal spacing from 10 to 15.4 Å with an intercalation rate of 86%, while FTIR and SEM confirmed structural reorganization and successful incorporation of phenylphosphonic functional groups. The modification increased interlayer accessibility and introduced additional P–OH active sites, enhancing hydrogen-bond donor density. Consequently, BPA6 achieved a maximum adsorption capacity of 123.3 $mg.g^{-1}$ at 55 °C, significantly exceeding raw bentonite. The kinetics were well described by the pseudo-second-order model, while the equilibrium data fit best with the Langmuir–Freundlich model. Thermodynamic analysis indicated a predominantly physisorption-driven process. BPA6 maintained stable performance over multiple regeneration cycles. Mechanistic insight was obtained by correlating spectroscopic, adsorption, and thermodynamic data, revealing a clear relationship between structure, surface chemistry, interactions, and performance. The adsorption mechanism is primarily governed by hydrogen bonding between Si–OH and intercalated P–OH moieties and the sulfonate and amine moieties of AO7. Phenylphosphonic acid intercalation optimizes clay surface chemistry, enhancing dye adsorption by BPA6 and highlighting its potential as a sustainable, high-performance wastewater adsorbent.

Keywords: Organobentonite; Phenylphosphonic acid; Characterization; Acid Orange 7; Adsorption; Mechanism

How to Cite: Mahrez, N., Belkacem, F. Z., Amar, A., Khelifa, M., Çoruh, A., Boucif, F., Bessaha, F., Marouf-Khelifa, K., Khelifa, A. (2026). Enhanced Acid Orange 7 Adsorption by a Novel Organophosphorus-Modified Bentonite: Performance and Mechanistic Insights. *Bulletin of Chemical Reaction Engineering & Catalysis*, 21 (3), 569-585. (DOI: 10.9767/bcrec.20675)

Permalink/DOI: https://doi.org/10.9767/bcrec.20675

1. Introduction

Synthetic dyes are widely used across industries such as textile, leather, paper, plastics, and cosmetics. Currently, over 10,000 dyes are produced globally, with an annual output exceeding 7×10^5 metric tons, highlighting their industrial significance [1]. The textile sector is a major contributor to industrial water pollution, responsible for about 20 % of the total. Annually, 40,000–50,000 tons of synthetic dyes are released into aquatic environments [2], of which 10–15 % fail to bind to the target materials and are discharged as liquid waste [3]. These persistent dyes reduce light penetration in water, hinder photosynthesis, and cause long-term environmental damage [4].

Acid Orange 7 (AO7), also known as Orange II, is an anionic dye widely used in industries,

* Corresponding Authors.
Email: aminekhelifadz@yahoo.fr (A. Khelifa)
amine.khalifa@univ-mosta.dz (A. Khelifa)

such as paper manufacturing, textile dyeing, leather processing, and the production of personal care products and detergents [5]. Its widespread use stems from its chemically stable structure and high water solubility, and it is frequently employed as a model pollutant in adsorption studies [6]. AO7 poses significant environmental hazards due to its stability and persistence in aquatic environments, which reduce dissolved oxygen and adversely affect aquatic organisms. Its degradation can also produce aromatic amines, which are toxic and potentially carcinogenic, further increasing environmental risks [7]. This azo dye also presents human health risks. Exposure may cause irritation of the skin, eyes, and respiratory system, and has been associated with genotoxicity and adverse effects on liver and kidney function [8].

Various chemical, physical, and biological methods have been applied for AO7 removal from contaminated water, including photocatalytic degradation [9], precipitation [10], electrochemical treatments [11], membrane filtration [12], and biological oxidation. Although these approaches can achieve satisfactory removal, their large-scale application is often limited by high operational costs [13]. Adsorption, in contrast, is widely used due to its high efficiency and relatively low cost [14], and is commonly employed for dye removal from wastewater [15]. It has been applied in both gaseous [16, 17] and aqueous [18, 19] phases using a variety of materials, including polymeric resins [20], activated carbon [21], zeolites [22], and metal oxides [23].

Clay materials are widely studied due to their low cost and natural abundance. Bentonite, primarily composed of montmorillonite (a 2:1 layered aluminosilicate), has favorable physicochemical properties but limited adsorption capacity in its natural form. This limitation can be overcome through organic intercalation, leading to organoclays with enhanced adsorption performance. These materials combine the properties of inorganic clay matrices with the hydrophobic character of organic components. While organoclays have been extensively investigated [24,25], the application of phenylphosphonic acid–modified 2:1 clays for pollutant removal remains unexplored.

The novelty of this work lies in the design of an innovative organobentonite obtained by intercalating phenylphosphonic acid into a 2:1 clay. Phenylphosphonic acid contains a P=O double bond and two P–OH groups, the latter enable strong and selective interactions with surface hydroxyls and pollutant molecules by acting as proton donors [26]. The phenyl ring imparts hydrophobic character to the modified clay, converting hydrophilic surfaces into organophilic environments and increasing affinity for organic pollutants. Economically, phenylphosphonic acid remains competitive with the commonly used intercalating agent HDTMA, with reported prices of 0.59 €.g^{-1} and 0.82 €.g^{-1}, respectively, for 100 g quantities at 98% purity (Merck/Sigma-Aldrich). Overall, it provides a balanced combination of molecular size and reactivity, enabling interlayer expansion, efficient removal of organic contaminants, and cost-effectiveness.

Bentonite was intercalated with phenylphosphonic acid (PA) to produce a novel organoclay, which was characterized by X-ray diffraction (XRD), scanning electron microscopy (SEM), and Fourier-transform infrared (FTIR) spectroscopy. Its adsorption of Acid Orange 7 was evaluated with respect to pH, temperature, contact time, and initial dye concentration. Four adsorption–desorption cycles were performed to assess reusability, and FTIR analysis before and after adsorption provided insights into the interaction mechanism between the dye and PA-modified bentonite.

2. Materials and Method

2.1. Materials and Synthesis

Raw bentonite, collected from a deposit in western Algeria (Mostaganem), was initially subjected to physicochemical characterization. The material was then chemically modified through intercalation with phenylphosphonic acid. The bentonite exhibited a cation exchange capacity (CEC) of 80 m_{eq}/100 g. The suspension was magnetically stirred at room temperature for 14 days, followed by vacuum filtration. The resulting organoclay was thoroughly washed, dried overnight at 70 °C, and stored for further experiments. A schematic representation of the synthesis of phenylphosphonic acid–intercalated bentonite is given in Figure 1. The modified clay was designated BPA6, where B, PA, and 6 refer to bentonite, phenylphosphonic acid, and a molar ratio six times the bentonite CEC, respectively. This designation is used consistently throughout the manuscript.

2.2. Characterizations

Powdered samples were characterized by X-ray diffraction (XRD) using a Bruker Advance D8 diffractometer with Cu-Kα radiation, scanning over a 2θ range of 2° to 70°. The surface morphology of both the raw bentonite and the modified BPA6 was examined by scanning electron microscopy (SEM) employing a JEOL JSM microscope at different magnifications. In addition, diffuse reflectance infrared Fourier transform (DRIFT) spectroscopy analyses were performed on a Bruker Alpha spectrometer equipped with a DTG detector. The DRIFT spectra

were recorded over the 4000–500 cm^{-1} range with a spectral resolution of 2 cm^{-1}.

2.3. Adsorption Testing

A standard stock solution of Acid Orange 7 (AO7, analytical grade, Fluka, Table 1) was prepared at a concentration of 1 $g.L^{-1}$. Adsorption experiments were carried out by contacting 0.020 g of the adsorbent with 0.020 L of AO7 solutions at predetermined concentrations, obtained by diluting the stock solution with distilled water. After centrifugation, the residual AO7

Table 1. Properties of Acid Orange 7 (AO7) and phenylphosphonic acid (PA).

Chemical product	Acid Orange 7 (AO7)
CAS number	633-96-5
Formula	$C_{16}H_{11}N_2NaO_4S$
Molecular weight (g.mol $^{-1}$)	350.32
Structure of Acid Orange 7 (AO7)	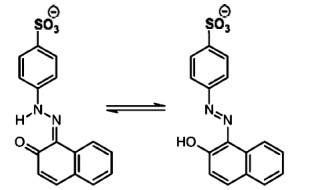 Hydrazone form Azo form
Chemical product	phenylphosphonic acid (PA)
CAS number	1571-33-1
Formula	$C_6H_5P(O)(OH)_2$
Molecular weight (g.mol^{-1})	158.09
Structure of phenylphosphonic acid (PA)	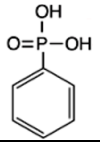

Figure 1. Schematic representation of the synthesis of phenylphosphonic acid–intercalated bentonite.

concentration in the supernatant was quantified using an Analytik Jena Specord 120 Plus UV–Vis spectrophotometer. All experiments were performed in triplicate at temperatures of 25, 40, and 55 °C. The experimental conditions are reported in Table 2.

3. Results and Discussion

3.1. Characterizations

3.1.1. X-ray diffraction analysis

The XRD patterns of untreated and phenylphosphonic acid–intercalated bentonites are shown in Figure 2. In raw bentonite (B), a basal reflection appears at 2θ ≈ 8.8°, corresponding to a *d*-spacing of approximately 10 Å for the (001) plane of pristine montmorillonite, denoted Im001. Montmorillonite is the predominant 2:1 clay mineral in bentonite. Another peak, labeled Im001h, is observed at 2θ = 6.8°, corresponding to a basal spacing of 13.0 Å, which is attributed to hydrated montmorillonite. A d-spacing of 13.0 Å is characteristic of montmorillonite containing a single interlayer water sheet [27].

The BPA6 sample exhibits a shift of the (001) reflection toward lower angles, from 8.8° to 5.7°, indicating an expansion of the montmorillonite interlayer distance [28]. This shift provides strong evidence for the successful intercalation of phenylphosphonic acid, as reflected by the appearance of the first-order basal reflection of the intercalated phase, denoted Ii001. Specifically, the organo-montmorillonite BPA6 displays a *d*-spacing of 15.4 Å (2θ = 5.7°), compared to 10 Å (2θ = 8.8°) for pristine montmorillonite (B). Additional reflections (Ii003 and Ii005), corresponding to the third and fifth basal orders, respectively, indicate the formation of an ordered intercalated structure. Non-basal reflections (Ii) were also observed. Furthermore, the presence of the Ik001 and Ik004 reflections suggests the persistence of a residual non-intercalated phase in BPA6 that does not participate in the intercalation process. Overall, these results indicate that the organobentonite is only partially intercalated.

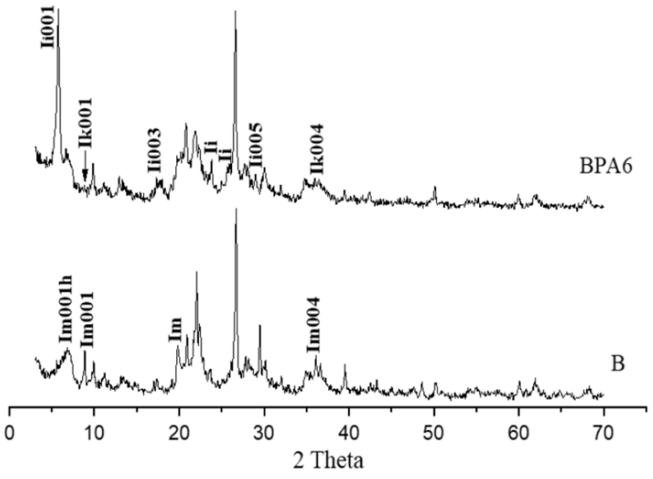

Figure 2. XRD diagrams of B, and BPA6 (B: Bentonite, PA: phenylphosphonic acid, 6: six times CEC) with: Im001h: first-order basal plane of the montmorillonite phase intercalated with one water layer; Im001: first basal reflection of B; Im004: fourth basal reflection of B; Im: non-basal reflection of B; Ii001: first basal reflection of the intercalated phase; Ii003: third basal reflection of the intercalated phase; Ii004: fourth basal reflection of the intercalated phase; Ii005: fifth basal reflection of the intercalated phase; Ii: non-basal reflection of the intercalated phase; Ik001: first basal reflection of the residual phase; Ik004: fourth basal reflection of the residual phase.

The degree of intercalation within the montmorillonite interlayer was quantified using the following equation:

$$IR = Ii001/(Ii001+Ik001) \quad (1)$$

where *IR* denotes the intercalation ratio, *Ii001* corresponds to the intensity of the first-order basal reflection of the intercalated fraction, and *Ik001* represents the intensity of the first-order basal reflection of the non-intercalated fraction.

The intercalated fraction was determined to be 86.2%, corresponding to an interlayer spacing of 15.4 Å. This result indicates that approximately 14% of the layers in BPA6 remain non-intercalated. The increase in basal spacing from 10 Å (d_0) to 15.4 Å (d) corresponds to an interlayer expansion of 5.4 Å due to intercalation. Assuming a molecular length of phenylphosphonic acid of ≈ 6 Å (L), as reported in crystallographic studies [29], the inclination angle (α) can be estimated using the relationship:

$$\sin(\alpha) = \frac{d-d_0}{L} \quad (2)$$

Table 2. Experimental conditions for the adsorption and desorption of Acid Orange 7.

Concentration	60, 80, 100, 150, 200, 300, 400, 500 mg.L^{-1}; contact time: 120 min; pH: 6; [solid]/[solution]: 1 g.L^{-1}
pH	2, 4, 6, 8, 10, 12; [solid]/[solution]: 1 g.L^{-1}; *T*: 25 °C; C_0 = 150 mg.L^{-1};
Time	contact time: 120 min 3, 5, 10, 20, 40, 60, 120, 240 min; C_0 = 150 mg.L^{-1} [solid]/[solution]: 1 g.L^{-1}; *T*: 25, 40 and 55 °C; pH: 6
Temperature	25, 40, 55 °C
Desorption	Eluents: NaOH; methanol; ethanol; butanol; water; [solid]/[solution]: 1 g.L^{-1}; C_0 = 500 mg L^{-1}; contact time: 120 min; *T*: 55 °C
Regeneration	4 cycles of adsorption/desorption; eluent: ethanol; *T*: 55 °C

This yields an angle α of 64∘ to the silicate surface (26° to the silicate surface normal), indicating a tilted orientation of the molecule within the interlayer space. Such configurations are commonly observed for small aromatic species confined in layered systems, where molecular orientation is governed by intermolecular interactions and steric constraints [30].

3.1.2. SEM analysis

The surface morphology of the untreated and phenylphosphonic acid–intercalated bentonite samples was characterized using scanning electron microscopy (SEM), as shown in Figure 3. Comparative SEM micrographs of the raw bentonite, B, and the intercalated bentonite, BPA6, recorded at different magnifications (10000×, 25000×, and 50000×), reveal morphological differences.

As evidenced by the SEM micrographs (Figure 3a,b), raw bentonite (B) exhibits a heterogeneous morphology characterized by aggregates of varying size and shape. These images also reveal irregularly shaped plate-like particles assembled into compact agglomerates

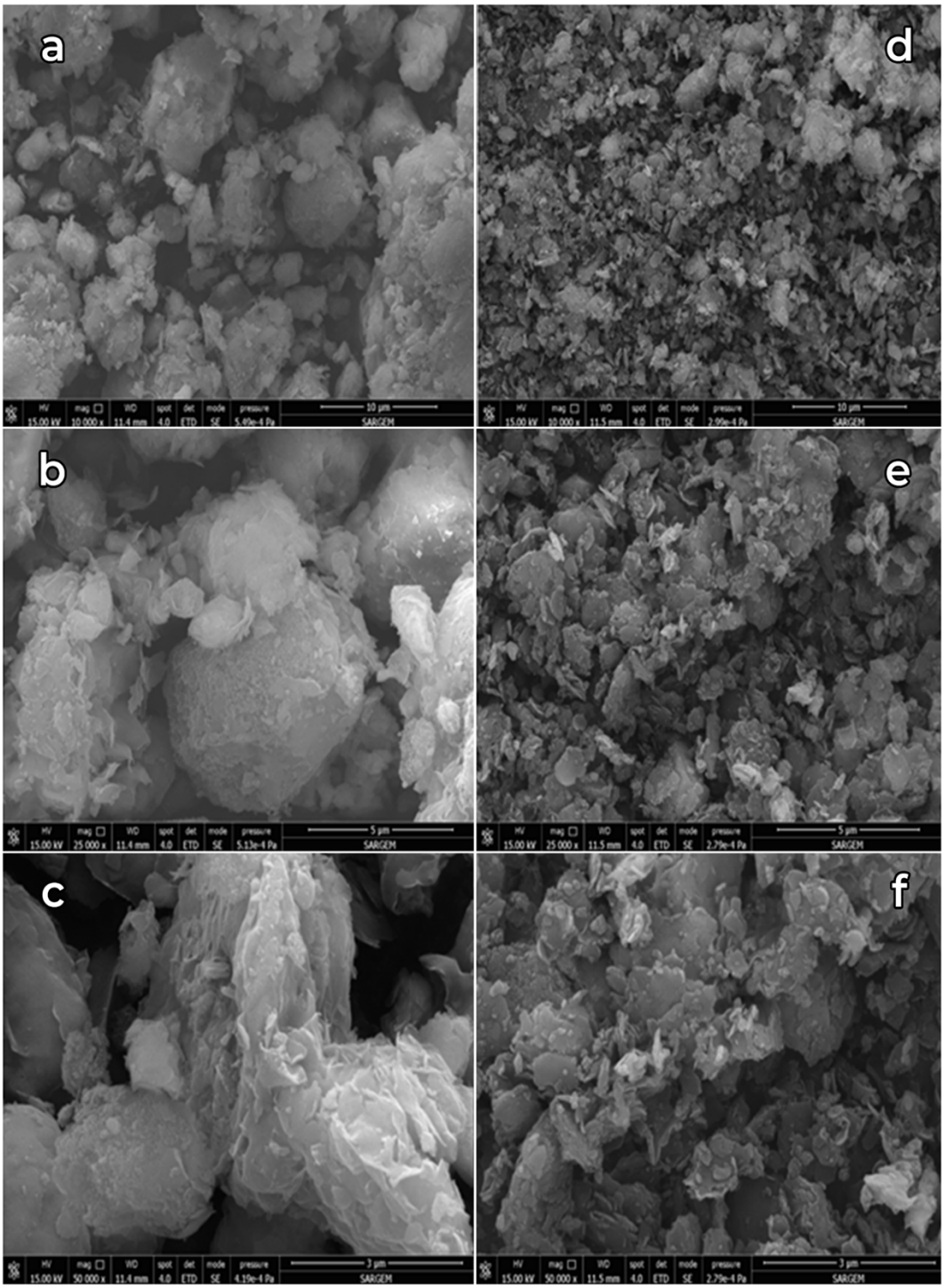

Figure 3. SEM images of untreated bentonite B (a: 10000×, b: 25000, and c: 50000×) and BPA6 (d: 10000×, e: 25000, and f: 50000×).

through the stacking of multiple flakes, resulting in a highly heterogeneous surface typical of natural bentonite materials [31]. SEM observations shows that the surface texture of the particles could not be clearly resolved in some areas, largely due to the magnification used and the tendency of particles to coalesce, which obscured fine morphological details. At higher magnification (50000×; Figure 3c), the micrograph reveals a stacked, sheet-like structure that is characteristic of layered clay materials [32].

The intercalation of phenylphosphonic acid into bentonite led to marked morphological changes. As illustrated in Figure 3d,e, both particle morphology and aggregation behavior were significantly altered, resulting in the formation of finer organobentonite particles. Intercalation within the bentonite interlayer space modifies the surface charge and hydrophobicity of the clay, rendering the particle surfaces less polar and weakening interparticle electrostatic interactions. As a result, compact agglomerates are reduced in favor of more dispersed, ultrafine structures [33]. At a magnification of 50000× (Figure 3f), HPA6 displays numerous small particles arranged into plate-like structures, forming thin, flat, and parallel layers characteristic of smectite-type clays [34].

3.2. Adsorption of Acid Orange 7

3.2.1. pH effect

The influence of pH on the adsorption of AO7 was investigated across a pH range of 2 to 12, as illustrated in Figure 4. The adsorption capacity increased markedly as the pH rose from 2 to 6, reaching a maximum at this value, where BPA6 reached an adsorption capacity of 29.1 $mg.g^{-1}$. Beyond pH 6, the adsorption capacity gradually decreased with increasing pH, reaching 16.9 $mg.g^{-1}$ at pH of 12, which suggests a reduced affinity between the adsorbent and the dye under alkaline conditions. Accordingly, pH of 6 was selected for subsequent experiments, as it corresponds to the optimal adsorption conditions [35]. According to Bessaha *et al.* [36], the bentonite used in the present work has a pzc of 7.8. Anionic dyes typically adsorb more efficiently at pH values below the pH_{pzc}, whereas cationic dyes are preferentially adsorbed at higher pH values. However, the adsorption maximum observed at pH of 6, close to the surface neutrality of the material, suggests that electrostatic interactions are not the dominant factor in AO7 adsorption. This conclusion is further supported by the low adsorption observed at pH of 2, where the material and AO7 are positively and negatively charged, respectively. BPA6 consistently exhibited a higher adsorption capacity than raw bentonite (B) over the entire pH range investigated. This highlights the beneficial role of phenylphosphonic acid intercalation in enhancing AO7 adsorption. The role of phenylphosphonic acid in adsorption is discussed in the interaction mechanism section.

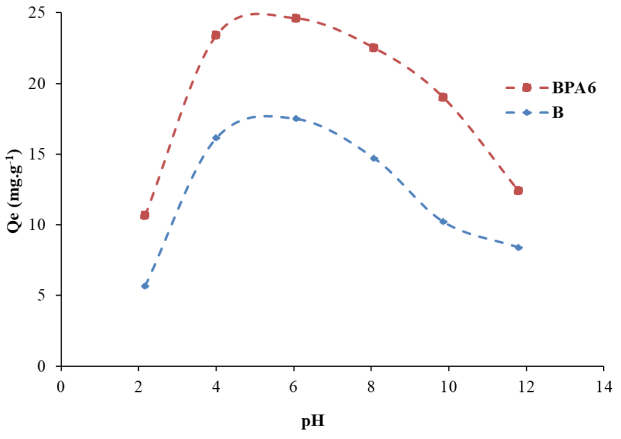

Figure 4. Effect of initial pH on the adsorption of AO7 by bentonite (B) and intercalated bentonite (BPA6).

3.2.2. Kinetics

Figure 5 illustrates the adsorption kinetics of AO7 onto B and BPA6. A rapid uptake occurred during the first 20 min, followed by a gradual decrease in the adsorption rate, reaching equilibrium after approximately 120 min. An equilibrium time of 120 min has been widely reported as adequate for various pollutant–adsorbent systems, such as Congo red–halloysite [37], catechol–dolomite [38], and Cr(VI)–zeolite [39]. The enhanced adsorption observed at the initial stage can be attributed to the high availability of active sites on the adsorbent surface, particularly for BPA6. An equilibrium time of 120 min was established as adequate for both materials. The equilibrium adsorption capacity of BPA6 was estimated at 19 $mg.g^{-1}$. Figure 5b depicts the effect of temperature on the adsorption kinetics of AO7 onto BPA6, revealing a marked improvement in adsorption efficiency with increasing temperature, as the uptake increased from 19 $mg.g^{-1}$ at 25 °C to 38 $mg.g^{-1}$ at 55 °C.

The kinetic parameters were determined by fitting the experimental data to various kinetic models, as summarized in Table 3. The pseudo-first-order model was not suitable for describing the obtained kinetic data, as evidenced by the low determination coefficients (R^2) and the significant discrepancy between experimental and theoretical adsorption capacities (Table 4). The results demonstrate that the adsorption of AO7 is well described by the pseudo-second-order model. The R^2 values exceeded 0.990, while an excellent agreement was found between experimental and

theoretical adsorption capacities. These findings suggest that the adsorption of AO7 is predominantly driven by interactions between the adsorbent and the adsorbate. The increase in the h value for BPA6 with rising temperature indicates a faster adsorption rate at the initial stage of the process. The intraparticle diffusion model fits the adsorption data for both B and BPA6, as indicated by the relatively high R^2 values in Table 4. The intraparticle diffusion constants ($k_i d$) for the intercalated material increase with increasing temperature, suggesting that diffusion within the pores is facilitated at higher temperatures. The Elovich kinetic model is commonly used to describe adsorption on heterogeneous surfaces, where variations in active sites and adsorption energies affect the process. The experimental data show a good fit with the Elovich model, indicating that the adsorption of AO7 is influenced by temperature.

3.2.3. Isotherms and affinity

The equilibrium adsorption isotherms of AO7 onto B and BPA6 are presented in Figure 6. For both adsorbents, the adsorption capacity increases with increasing temperature, indicating an endothermic process. In the case of raw bentonite, adsorption capacities of 50.6 $mg.g^{-1}$ and 81.3 $mg.g^{-1}$ were obtained at 25 and 55 °C, respectively. BPA6 demonstrates superior adsorption performance, with capacities of 53.7 $mg.g^{-1}$ and 123.3 $mg.g^{-1}$ at 25 and 55 °C, respectively. This improvement, particularly at 55 °C, highlights the positive role of phenylphosphonic acid incorporation, which enhances the availability of surface sites and strengthens their interaction with AO7 species.

Figure 7 illustrates the adsorption behavior of B and BPA6 toward AO7 at 55 °C. Compared with raw bentonite, BPA6 exhibits a markedly greater affinity for AO7 molecules. The maximum

Table 3. Pseudo-first order, pseudo-second order, intraparticle diffusion and Elovich models and their parameters.

Models and equations	Parameters
Pseudo-first order model [40]: $Q_t = Q_e(1 - exp(k_1 t))$ (3)	Q_e: amount adsorbed at equilibrium ($mg.g^{-1}$) Q_t: amount adsorbed at time t ($mg.g^{-1}$) k_1: pseudo-first order rate constant (min^{-1}) t: contact time (min)
Pseudo-second order model [41]: $Q_t = \frac{t}{(\frac{1}{h})+(\frac{t}{Q_e})}$ (4) $h = k_2 Q_e^2$ (5)	k_2: pseudo-second order rate constant ($g.mg^{-1}.min^{-1}$) h: initial adsorption rate ($mg.g^{-1}.min^{-1}$)
Intraparticle diffusion rate model [42]: $Q_t = k_{id} t^{1/2} + C$ (6)	k_{id} : intraparticle diffusion rate constant ($mg.g^{-1}.min^{-1/2}$) C : constant ($(mg.g^{-1})$
Elovich model [43]: $Qt = \frac{1}{\beta}\ln(\alpha\beta) + \frac{1}{\beta} ln\, t$ (7)	α : initial adsorption rate ($mg.g^{-1}.min^{-1}$) β : desorption constant ($g.mg^{-1}$)

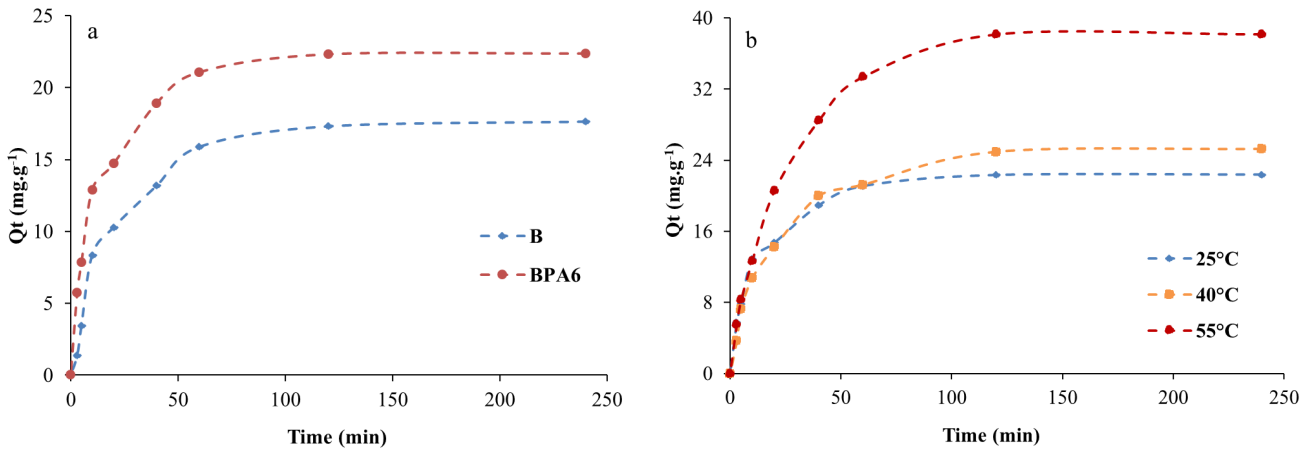

Figure 5. Adsorption kinetics of AO7 by: (a) bentonite (B) and intercalated bentonite (BPA6) at 25 °C; (b) BPA6 at 25, 40, and 55 °C.

adsorption capacities reached 81.3 mg.g^{-1} for B and 123.3 mg.g^{-1} for BPA6. This improved performance can be ascribed to the intercalation of phenylphosphonic acid (PA) within the interlayer space of bentonite, which promotes stronger interactions between the modified surface and AO7 species. The presence of intercalated PA likely enhances the interfacial forces governing the adsorption process, thereby contributing to the higher uptake observed for BPA6. In a previous study, the POH group of PA was shown to act as a hydrogen-bond donor, while an oxygen atom from a neighboring species serves as the corresponding hydrogen-bond acceptor [44].

3.2.4. Comparison of adsorption capacity with other adsorbents

The adsorption efficiency of BPA6 toward AO7 was evaluated and compared with that of various adsorbent materials reported in the literature. As shown in Table 5, BPA6 exhibits an adsorption capacity of 123.38 mg.g^{-1}, significantly exceeding those reported for other clay based–materials, including montmorillonite, palygorskite, and sepiolite. This enhanced performance highlights the effectiveness of the synthesis method, as BPA6 outperforms other clays prepared or modified via alternative approaches.

3.2.5. Equilibrium isotherm modeling

The experimental equilibrium data were fitted using several commonly applied isotherm models in order to better elucidate the adsorption behavior of the studied systems. The selected models and their corresponding parameters are summarized in Table 6. Model performance was evaluated based on the coefficient of determination (R^2), the mean relative error (E, %), and the agreement between the calculated and experimentally determined maximum adsorption capacities. The fitting results are compiled in Table 7.

The Langmuir model provides an unsatisfactory description of the experimental data, as indicated by low R^2 values for all adsorbents. In addition, this model predicted maximum adsorption capacities (Q_m) that were

Table 5. Comparison of adsorption capacity of Acid Orange 7 for different clay-based materials.

Adsorbents	Q_{max} (mg.g^{-1})	Ref.
Methylimidazolium modified–MMT	2.3	[45]
Cetylpyridinium-montmorillonite	16.96	[46]
HDTMA-montmorillonite	58.20	[47]
DMDOA-palygorskite	96.15	[48]
ODTMA-palygorskite	99.01	[48]
Sepiolite	110.05	[49]
Untreated bentonite	81.35	Present study
BPA6	123.38	Present study

Table 6. Langmuir, Freundlich and Langmuir-Freundlich isotherms and their parameters.

Models and equations		Parameters
Langmuir isotherm [50]: $Q_e = Q_m \frac{K_L C_e}{1+K_L C_e}$	(8)	Qe: amount adsorbed at equilibrium (mg.g^{-1}) C_e: concentration at equilibrium (mg.L^{-1}) K_L : affinity parameter (L.mg^{-1}) Qm: quantity fixed in monolayer (mg.g^{-1})
Freundlich isotherm [51]: $Q_e = K_F C_e^{\frac{1}{n}}$	(9)	K_F: factor correlated with adsorption capacity (L.g^{-1}) $1/n$: factor due to the intensity of adsorption
Langmuir–Freundlich [52]: $Q_e = \frac{K_{LF} C_e^{\beta}}{1+a_{LF} C_e^{\beta}}$	(10)	K_{LF}: The Langmuir–Freundlich equilibrium isotherms constant (L.g^{-1}) $^{-\beta}$ a_{LF} : Constant (L.mg^{-1}) $^{-\beta}$ β: factor correlated to surface heterogeneity

Table 4. Kinetic parameters for Acid Orange 7 adsorption by B and BPA6 at different temperatures.

Samples			Pseudo-first-order model			Pseudo-second-order model				Intra-particle diffusion			Elovich Model		
	T (°C)	Q_{eexp} (mg.g^{-1})	Q_{ecal} (mg.g^{-1})	k_1 (min^{-1})	R^2	Q_{ecal} (mg.g^{-1})	h (mg.g^{-1}. min^{-1})	k_2 (g.mg^{-1} . min^{-1})	R^2	k_{id} (mg.g^{-1}. min$^{-1/2}$)	l (mg.g^{-1})	R^2	α (mg.g^{-1}. min^{-1})	β (g.mg^{-1})	R^2
B	25	18.28	12.22	0.024	0.877	20.08	1.28	0.0032	0.998	1.633	4.06	0.997	3.10	0.253	0.959
BPA6	25	19.12	11.96	0.024	0.849	20.37	1.54	0.0037	0.996	1.740	3.78	0.969	4.69	0.274	0.923
	40	24.90	18.53	0.026	0.976	27.17	1.71	0.0023	0.999	2.397	3.51	0.965	4.16	0.190	0.976
	55	38.13	33.33	0.030	0.996	41.84	2.18	0.0012	0.998	4.468	0.10	0.988	4.98	0.118	0.969

Table 7. Isotherm parameters for the Langmuir, Freundlich and Langmuir-Freundlich models for the adsorption of AO7 by B and BPA6.

Material	T (°C)	Langmuir model				Freundlich model				Langmuir–Freundlich model				
		Q_m (mg/g)	K_L (L/mg)	R^2	E_{rm} (%)	K_F (L/g)	n	R^2	E_{rm} (%)	K_{LF} (L/g)$^{-\beta}$	β	a_{LF} (L/mg)$^{-\beta}$	R^2	E_{rm} (%)
B	25	169.49	0.0009	0.579	8.5	0.32	1.19	0.984	8.2	0.1492	1.001	0.0003	0.999	8.6
	40	-3333	-5.5186	0.002	10.3	0.22	1.03	0.971	9.7	0.113	1.102	0.00006	0.999	9.9
	55	-384.6	0.0003	0.039	14.9	0.29	1.06	0.950	8.9	0.3292	0.96	0.0008	0.999	10.3
BPA6	25	111.11	0.0022	0.961	4.2	0.54	1.30	0.985	6.4	0.1622	1.09	0.0016	0.999	4.5
	40	588.24	0.0004	0.267	6.2	0.35	1.10	0.989	5.9	0.1907	1.034	0.0001	0.995	7.3
	55	161.29	-0.0008	0.233	15.2	0.16	0.87	0.966	9.0	0.1540	1.2	0.0002	0.999	11.5

physically unrealistic, with some yielding negative values. Taking into account adsorption kinetics, solution pH, and adsorbate–adsorbent affinity, the findings indicate that adsorption occurs on sites with heterogeneous energy, deviating from the assumptions of the Langmuir model. The Freundlich model generally fits the experimental data well, although some R^2 values are somewhat low. Its main limitation lies in its inability to predict a finite adsorption capacity at high equilibrium concentrations. The Langmuir–Freundlich model, which incorporates three fitting parameters, is well suited for describing adsorption on both homogeneous and heterogeneous surfaces. Table 7 shows that the Langmuir–Freundlich model accurately describes the experimental isotherms for both B and BPA6, with a coefficient of determination (R^2) of 0.99 and low mean errors. The model parameters a_{LF}, β, and K_{LF} were employed to obtain theoretical isotherms, which were subsequently compared with the experimental data (Figure 6). A close agreement was observed between the calculated and measured adsorption profiles.

3.2.6. Thermodynamic properties

Enthalpy ($\Delta H°$), entropy ($\Delta S°$), and Gibbs energy ($\Delta G°$) were determined using the equations below:

$$\ln(K_d) = (-\Delta H°/R \times T) + (\Delta S°/R) \quad (11)$$

$$K_d = 1000*(Q_e/C_e) \quad (12)$$

$$\Delta G° = \Delta H° - T.\Delta S° \quad (13)$$

with K_d is distribution coefficient ($L.g^{-1}$), $\Delta H°$ is enthalpy ($kJ.mol^{-1}$), $\Delta S°$ is entropy ($kJ.mol^{-1}.K^{-1}$), $\Delta G°$ is Gibbs free energy ($kJ.mol^{-1}$), and T is absolute temperature (K).

Table 8 presents the thermodynamic parameters related to AO7 adsorption. The negative values of $\Delta G°$ indicate that the adsorption occurs spontaneously. For both B and BPA6, the magnitude of $\Delta G°$ rises with increasing temperature, suggesting that higher thermal energy favors the process. $\Delta G°$ values below −20 $kJ.mol^{-1}$ are often associated with physisorption [53]. However, this threshold should not be considered definitive. The positive $\Delta H°$ values show that AO7 adsorbs onto both B and BPA6 through an endothermic process. Similarly, $\Delta H°$ values under 84 $kJ.mol^{-1}$ are generally consistent with physisorption [54]. This implies that the adsorption is reversible, allowing regeneration of BPA6 after AO7 removal. Overall, these results support the predominance of physisorption, likely

Table 8. Thermodynamic parameters for the adsorption of AO7 onto B and BPA6.

Sample	$\Delta H°$ ($kJ.mol^{-1}$)	$\Delta S°$ ($kJ.mol^{-1}.K^{-1}$)	$\Delta G°$ ($kJ.mol^{-1}$)		
			25 °C	40 °C	55 °C
B	14.94	0.09	-11.85	-13.20	-14.54
BPA6	27.16	0.13	-11.89	-13.85	-15.82

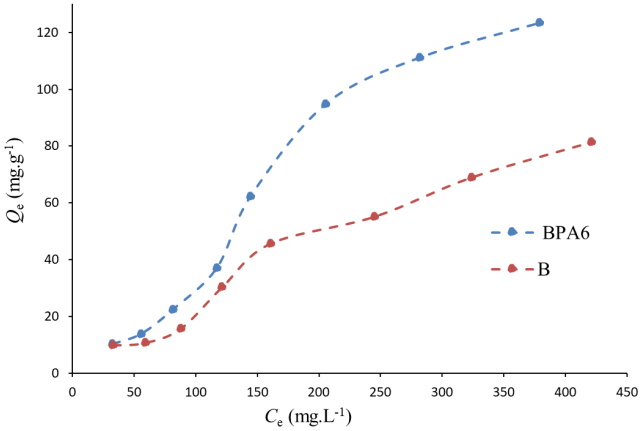

Figure 7. Affinity of bentonite (B) and intercalated bentonite (BPA6) toward AO7, at 55 °C.

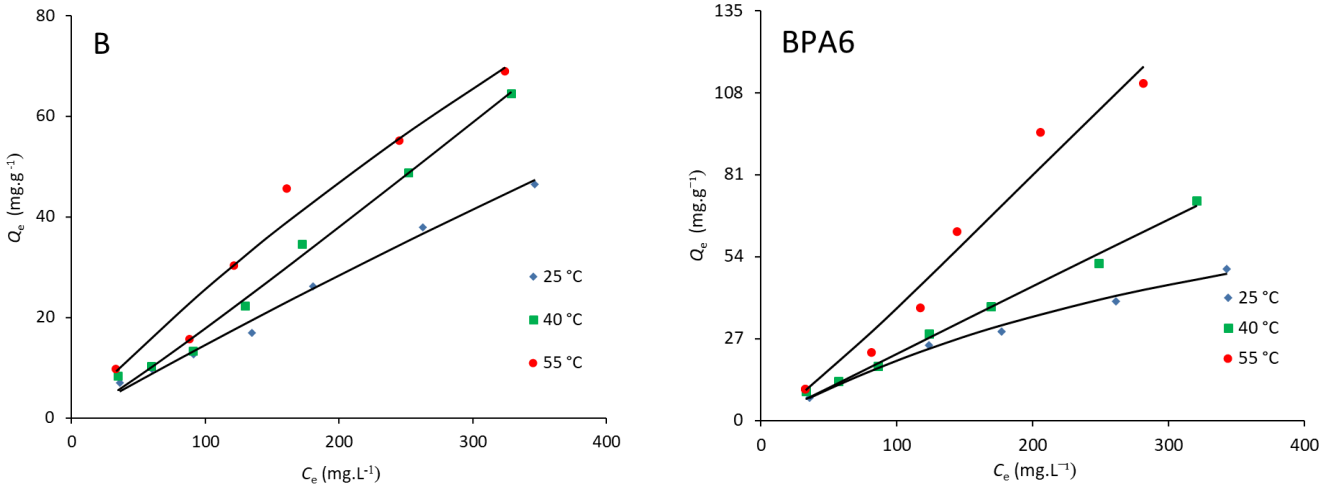

Figure 6. Isotherms according to the experimental data (…) and Langmuir-Freundlich model (—) for B and BPA6.

involving weak interactions such as hydrogen bonding [55]. The positive $\Delta S°$ values are likely due to the breakdown of the AO7's hydration shell and the simultaneous release of water molecules from the organobentonite surface, during the transfer of AO7 onto BPA6 [56]. This increase in disorder ($\Delta S°>0$) contributes to the thermodynamic driving force for spontaneous adsorption ($\Delta G°<0$).

3.2.7. Desorption and reusability

The desorption of AO7 from BPA6 was investigated using five eluents: NaOH, water, butanol, ethanol, and methanol as illustrated in Figure 8. Among these, ethanol proved to be the most effective, enabling the recovery of up to 60% of the adsorbed dye. the desorption efficiency followed the order: ethanol (60%) > methanol (52%) > butanol (42.2%) > water (20%) > NaOH (19.8%). Hydrophilic (–NH, $–SO_3^-$) and hydrophobic alkyl groups of AO7 interact selectively with the hydroxyl and alkyl moieties of alcohols, promoting desorption from AO7–loaded bentonite [57]. Ethanol, with its moderately sized hydrocarbon chain, forms effective hydrophobic interactions with the alkyl groups of AO7, thereby disrupting dye–phenylphosphonic acid associations. In contrast, methanol is too polar to compete with these interactions, while butanol, despite its higher hydrophobicity, is limited by restricted accessibility. Desorption can be described as a coupled diffusion–interaction process. Due to its intermediate molecular size, ethanol readily diffuses into the organobentonite interlayers, whereas butanol is sterically hindered and methanol interacts only weakly with the hydrophobic phase. Water exhibits poor desorption efficiency because of its low affinity for the organic phase of BPA6, which limits AO7 extraction from the clay galleries. Overall, ethanol achieves the best performance by balancing hydrophobicity and accessibility within the bentonite structure. Its efficiency arises from the combined effects of rapid diffusion and strong interactions with the adsorbed dye.

Given the importance of regenerability for practical applications, four successive adsorption–desorption cycles were conducted using ethanol as the eluent (Figure 9). After each desorption step, the solution was analyzed using UV–Vis spectroscopy from 200 to 600 nm, which revealed no distinct features attributable to the release of phenylphosphonic acid. The reusability of the material was assessed through its adsorption performance over multiple cycles, without monitoring its cation exchange capacity (CEC) after each adsorption–desorption step. The relatively stable adsorption capacity observed during the first three cycles indicates that the material largely retains its functionality upon recycling, although CEC measurements would be required to confirm this observation.

BPA6 maintained its adsorption capacity over the first three cycles, but a marked decline was observed in the fourth cycle, where the capacity dropped to 15%. This decrease is likely due to cumulative material loss during regeneration, as well as the progressive accumulation of AO7 on the surface, which partially blocked active sites and reduced accessibility [58]. Such a decline illustrates a common limitation in the long-term regenerability of adsorbents, often caused by incomplete desorption and progressive pore fouling. While solvent-based regeneration can provide good initial recovery, repeated cycles may lead to performance deterioration due to blocked micropores or strongly bound adsorbates. Future studies should focus on optimized regeneration strategies, such as alternative eluents or hybrid approaches, to enhance desorption efficiency and extend adsorbent lifetime [59].

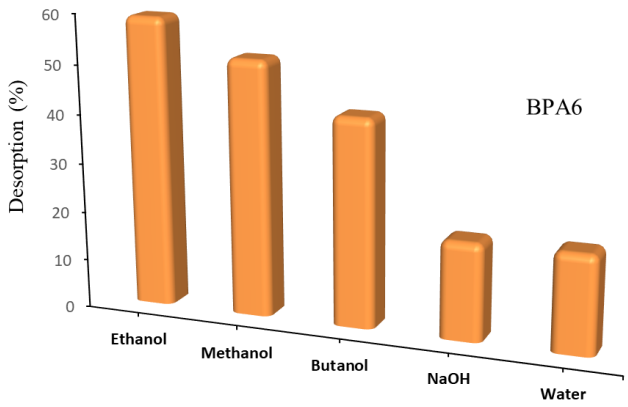

Figure 8. Desorption of AO7 from BPA6 with different eluents, at 55 °C.

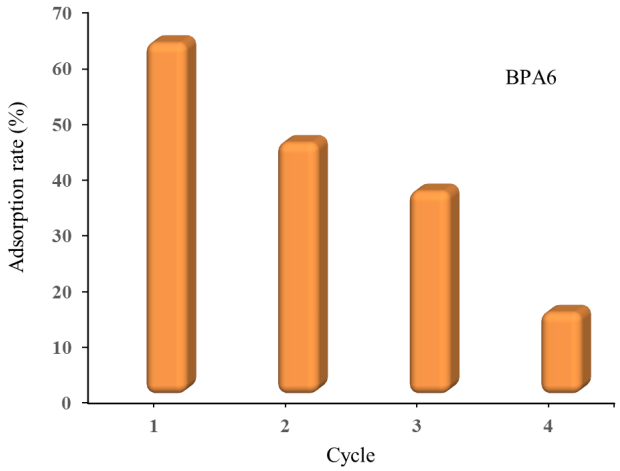

Figure 9. Adsorption rate of BPA6 toward AO7 using ethanol as the eluent over successive cycles at 55 °C.

3.3. FTIR Analysis

Figure 10 depicts the IR spectra of intercalated bentonite (BPA6), acid orange 7 (AO7), and AO7 adsorbed on intercalated bentonite (AO7/BPA6). The peak at 3623 cm^{-1} corresponds to the –OH stretching of structural hydroxyls (Figure 10–BPA6). The absence of a broad band around 3400 cm^{-1}, attributed to hydrogen-bonded interlayer water, indicates that the interlayer water has been displaced by the intercalated phenylphosphonic acid. These results indicate that modification of bentonite with phenylphosphonic acid has changed its surface properties from hydrophilic to hydrophobic [60]. The smooth peak at 1635 cm^{-1} is associated with the H–O–H bending of water molecules retained within the silica matrix. The bands at 1199 cm^{-1} and 1160 cm^{-1} correspond to the P=O and P–O stretching vibrations, respectively [61]. Additional vibrations are observed at νas, P–OH (920 cm^{-1}) and νs, P–OH (834 cm^{-1}) [62,63]. These phosphorus-related spectral features clearly show that phenylphosphonic acid has been successfully intercalated between the bentonite layers. The intense band at 1011 cm^{-1} is assigned to the Si–O stretching vibration in the tetrahedral sheet. The band at 796 cm^{-1} arises from Si–O bending, while the band at 691 cm^{-1} corresponds to the Si–O–Al bending mode [64].

Acid Orange 7 undergoes azo–hydrazone tautomerism (Table 1), a structural feature commonly observed in phenylazonaphthol dyes. The FTIR spectrum of AO7 prior to adsorption is shown in Figure 10–AO7. The broad band at 3416 cm^{-1} is assigned to N–H stretching. The bands at 1551 and 1621 cm^{-1} are attributed to coupled vibrations involving N–H bending and –N=C stretching of the (NH–N=C) group, and to phenyl ring vibrations combined with C=N stretching, respectively [65]. The peak at 1502 cm^{-1} is ascribed to N–H bending vibration. The identification of the N–H and –N=C functional groups confirms that AO7 is present in its hydrazone form. NMR spectroscopy has revealed that AO7 predominantly adopts the hydrazone tautomeric form in aqueous solution [66]. The bands at 1593 and 1448 cm^{-1} are characteristic of phenyl ring vibrations. The bands at 1176 and 1115 cm^{-1} are associated with νas ($–SO_3^-$) and νs ($–SO_3^-$), respectively [65]. The presence of sulfonate ($–SO_3^-$) groups bonded to the aromatic rings is evidenced by bands at 1032, 695, and 617 cm^{-1}, which are assigned to the S=O, S–O, and S–C stretching modes, respectively [67].

After adsorption of acid orange 7 (Figure 10–AO7/BPA6), marked spectral changes occurred, including the disappearance of certain bands and the shift or appearance of others, indicating interactions between AO7 and the BPA6 organobentonite. The band at 3416 cm^{-1} changed in intensity, broadened and shifted to 3428 cm^{-1}, consistent with hydrogen-bond formation between the amine groups of the hydrazone form of AO7 and proton donors. This is further supported by the shift of the N–H bending band from 1502 to 1506 cm^{-1}. The bands attributed to the –N=C group, coupled with the phenyl ring and N–H, shifted from 1621 to 1618 cm^{-1} and from 1551 to 1538 cm^{-1}, respectively. Phosphorus-related bands: νP=O (1199 cm^{-1}), νP–O (1160 cm^{-1}), νas, P–OH (920 cm^{-1}), and νs, P–OH (834 cm^{-1}), shifted and/or changed in intensity after adsorption to 1203, 1161, 915, and 837 cm^{-1}, respectively. These observations suggest that phenylphosphonic acid intercalated within the bentonite layers may interact with AO7

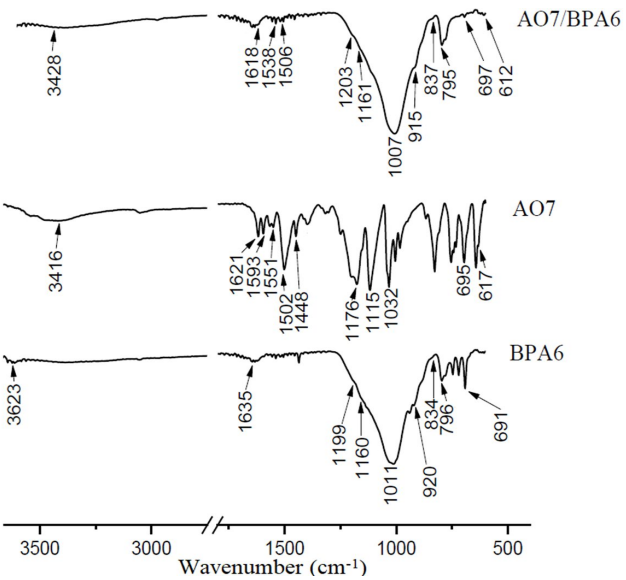

Figure 10. FTIR spectra of BPA6, AO7, and AO7-loaded BPA6 (AO7/BPA6).

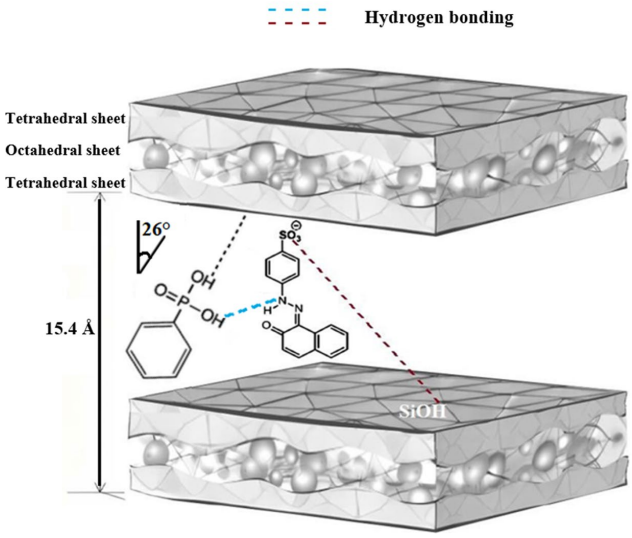

Figure 11. Proposed interaction mechanism between acid orange 7 and phenylphosphonic acid–intercalated bentonite (BPA6).

molecules via hydrogen bonding mediated by its P–OH group.

Noticeable shifts were observed in the $–SO_3^-$ bands after AO7 adsorption: ν_{as} ($–SO_3^-$) (from 1176 cm^{-1} to 1161 cm^{-1}), $\nu_{S=O}$ (from 1032 cm^{-1} to a band overlapping with $\nu_{Si–O}$ at 1007 cm^{-1}), $\nu_{S–O}$ (from 695 cm^{-1} to a band overlapping with $\delta_{Si–O}$ at 697 cm^{-1}), and $\nu_{S–C}$ (from 617 cm^{-1} to 612 cm^{-1}). These changes highlight the prominent role of the sulfonate group in the adsorption mechanism. The Si–O bands of the tetrahedral sheet also exhibited shifts: $\nu_{Si–O}$ (from 1011 cm^{-1} to a band overlapping with $\nu_{S=O}$ at 1007 cm^{-1}), $\delta_{Si–O}$ (from 796 cm^{-1} to 795 cm^{-1}), and $\delta_{Si–O}$ (from 691 cm^{-1} to a band overlapping with $\nu_{S–O}$ at 697 cm^{-1}). Such interactions between these functional groups are discussed further in the mechanism section.

3.4. Interaction Mechanism

The adsorption process is largely driven by hydrogen bonding, as indicated by IR spectroscopy and adsorption data. Intermolecular hydrogen bonds form between phenylphosphonic acid in the bentonite interlayer and the amine groups of AO7's hydrazone form, with POH groups acting as hydrogen-bond donors. Increasing intercalation incorporates more P–O–H groups, enhancing AO7 adsorption via hydrogen bonding and explaining the higher performance of BPA6. Previous work confirmed the POH group acts as a hydrogen-bond donor [44]. Evidence for amine involvement includes broadening of the 3416 cm^{-1} band and blue shifts at 3416 and 1502 cm^{-1}, corresponding to N–H stretching and bending modes, respectively. Such blue shifts reflect increased electron density around nitrogen, due to strengthened N···HX interactions and simultaneous weakening of the H-donor bond [65,68]. Consistent with Khezami *et al.* [69], amines typically act as hydrogen-bond acceptors in interactions with hydroxyl groups [70].

When dispersed in water, bentonite surface oxide groups hydrolyze to form silanol (Si–OH) and aluminol (Al–OH) groups, with neutral sites predominating near the point of zero charge (pzc) [71]. Given that the pzc of the bentonite is 7.8 [36] and the experiments were conducted at a similar pH, the tetrahedral sheet is primarily composed of Si–OH groups. IR spectroscopy shows shifts in Si–O bands after adsorption, indicating the involvement of silanol groups, which act as hydrogen-bond donors due to their slightly acidic character. This role is further supported by NMR results confirming the strong donor ability of Si–OH groups [72]. The participation of AO7, in its hydrazone form, is evidenced by changes in the vibrational bands of its $–SO_3^-$ group (S=O, S–O, and S–C), indicating its involvement in adsorption. As electron-rich species, sulfonate groups act as effective hydrogen-bond acceptors, forming interactions with Si–OH groups [73,74]. Overall, these interactions are consistent with hydrogen bonding between Si–OH and $–SO_3^-$ groups, as supported by both spectroscopic data and $\Delta H°$ values within the expected range for such interactions [55].

The enhanced adsorption of AO7 molecules by BPA6, compared to unmodified bentonite, is attributed to the involvement of intercalated –POH groups. In contrast, as mentioned above, the hydrolyzed surface of bentonite is primarily composed of silanol (Si–OH) groups [71], which act as the main active sites. The latter facilitate hydrogen bonding with the sulfonate and/or amine groups of AO7 in its hydrazone form. Among the available interactions, π–π stacking is well-established in biology, chemistry, and materials science, and often governs the adsorption of aromatic compounds onto carbon-based materials, polymers, and metal–organic frameworks (MOFs) [75]. In organoclays, however, its contribution appears more limited. Similarly, the involvement of exchangeable cations in electrostatic bonding is unlikely in smectitic clays, as these cations are surrounded by hydration shells that reduce direct interactions as hydration increases [76]. Based on intercalation characterization, AO7 adsorption results, and spectroscopic data, a mechanism for AO7 interaction with BPA6 is proposed (Figure 11).

4. Conclusion

In this study, a novel organobentonite (BPA6) was synthesized via intercalation of phenylphosphonic acid into bentonite, as confirmed by XRD, SEM, and FTIR analyses. The basal spacing increased from 10 Å to 15.4 Å, with an intercalated fraction of 86%. BPA6 exhibited superior adsorption of Acid Orange 7 compared with raw bentonite, achieving a maximum capacity of 123.3 mg g^{-1} at 55 °C. Adsorption was strongly influenced by pH, temperature, and contact time, following pseudo-second-order kinetics and a Langmuir–Freundlich isotherm. Thermodynamic analysis indicated spontaneous, endothermic, and predominantly physisorption-driven interactions, with hydrogen bonding between P–OH and Si–OH of BPA6 and the sulfonate and amine groups of AO7 as the primary adsorption mechanism. BPA6 also demonstrated good reusability over three cycles using ethanol as the eluent. These results highlight phenylphosphonic acid–modified bentonite as a cost-effective and efficient adsorbent for azo dyes, with promising applications in wastewater treatment and environmental remediation.

CRedit Author Statement

Author Contributions: Nouria Mahrez: Conceptualization, Formal analysis, Methodology; Fatima Zohra Belkacem: Data curation, Methodology, Investigation; Amine Amar: Investigation, Software; Mounir Khelifa: Supervision, Visualization; Ali Coruh: Supervision, Resources; Fatima Boucif: Visualization, Validation; Fatiha Bessaha: Validation, Writing – original draft; Kheira Marouf-Khelifa: Writing - Review & Editing, Resources; Amine Khelifa: Project administration, Review and Editing. All authors have read and agreed to the published version of the manuscript.

References

[1] Sahu, A., Poler, J.C. (2024). Removal and degradation of dyes from textile industry wastewater: Benchmarking recent advancements, toxicity assessment and cost analysis of treatment processes. *Journal of Environmental Chemical Engineering*, 12(5), 113754. DOI: 10.1016/j.jece.2024.113754

[2] Kavitha, G., Govindhan, M., Premkumar, S. (2025). Dye pollution and its implications for human health, aquatic ecosystems, and sustainable wastewater treatment: A comprehensive review. *Journal of Water Process Engineering*, 80, 109071. DOI: 10.1016/j.jwpe.2025.109071

[3] Sudarshan, S., Harikrishnan, S., Rathi Bhuvaneswari, G., Alamelu, V., Aanand, S., Rajasekar, A., Govarthanan, M. (2023). Impact of textile dyes on human health and bioremediation of textile industry effluent using microorganisms: Current status and future prospects. *Journal of Applied Microbiology*, 134, 1–23. DOI: 10.1093/jambio/lxac064

[4] Kumar, M., Mishra, A., Patel, S.K., Kushwaha, J., Singh, S., Mishra, V., Singh, D., Singh, V., Giri, B.S., Singhania, R.R., Singh, D. (2025). Environmental impacts and strategies for bioremediation of dye-containing wastewater. *Bioengineering*, 12, 1043. DOI: 10.3390/bioengineering12101043

[5] Cai, J., Xie, Q., Ding, Z., Cao, J., Liu, J., Xia, J., Yang, J. (2024). Enhanced mechanism of AO7 degradation by electrochemical activation of persulfate at carbon felt and electrogenerated H_2O_2 carbon black modified cathodes in divided cell. *International Journal of Electrochemical Science*, 12, 100861. DOI: 10.1016/j.ijoes.2024.100861

[6] Strebel, A., Behringer, M., Hilbig, H., Machner, A., Helmreich, B. (2024). Anionic azo dyes and their removal from textile wastewater through adsorption by various adsorbents: A critical review. *Frontiers in Environmental Engineering*, 3, 1347981. DOI: 10.3389/fenve.2024.1347981

[7] Vieira, J.C.B., Frizzo, C.P., de Sousa, H.C., Dias, A.M.A., Pereira, J.F.B. (2026). Adsorption of dyes from aqueous solutions using chitosan-based materials functionalized with ionic liquids: Acid Orange 7 as a case-of-study. *International Journal of Biological Macromolecules,* 342, 150287. DOI: 10.1016/j.ijbiomac.2026.150287

[8] Yoon, S., Calvo, J.J., So, M.C. (2018). Removal of Acid Orange 7 from aqueous solution by metal-organic frameworks. *Crystals*, 9(1), 17. DOI: 10.3390/cryst9010017

[9] Bellettini, G.C., Souza-Pereira, M., Benetti, R. M., Elyseu, F., Dal-Bó, A.G., Bernardin, A.M. (2026). Stress test of magnetite nanoparticles synthesized by controlled precipitation for the degradation of dyes under UV and visible radiation. *Materials Chemistry and Physics*, 348(1), 131626. DOI: 10.1016/j.matchemphys.2025.131626

[10] Tang, H., Wu, Z., Zhang, J., Su, R., Zhu, X., Dong, Z. (2025). Novel synthesis of nano-cerium oxide using ultrasonic microreactor: Process optimization and AO7 degradation. *Ceramics International*, 51(3), 3283–3292. DOI: 10.1016/j.ceramint.2024.11.307

[11] Baghani, M., Soltanian, M., Sarrafzadeh, M.H. (2026). Energy optimization in electrochemical oxidation for wastewater treatment using interpretable machine learning. *Chemical Engineering Journal Advances*, 25, 101044. DOI: 10.1016/j.ceja.2026.101044

[12] Liang, P., Rivallin, M., Cerneaux, S., Lacour, S., Petit, E., Cretin, M. (2016). Coupling cathodic Electro-Fenton reaction to membrane filtration for AO7 dye degradation: A successful feasibility study. *Journal of Membrane Science*, 510, 182–190. DOI: 10.1016/j.memsci.2016.02.071

[13] Ali, K., Zeidan, H., Ben Amar, R. (2023). Evaluation of the use of agricultural waste materials as low-cost and ecofriendly sorbents to remove dyes from water: A review. *Desalination and Water Treatment*, 302, 231–252. DOI: 10.5004/dwt.2023.29725

[14] Cheng, S., Zhao, S., Xing, B., Liu, Y., Zhang, C., Xia, H. (2022). Preparation of magnetic adsorbent-photocatalyst composites for dye removal by synergistic effect of adsorption and photocatalysis. *Journal of Cleaner Production*, 348, 131301. DOI: 10.1016/j.jclepro.2022.131301

[15] Crini, G. (2006). Non-conventional low-cost adsorbents for dye removal: A review. *Bioresource Technology*, 97(9), 1061–1085. DOI: 10.1016/j.biortech.2005.05.001

[16] Bendenia, S., Marouf-Khelifa, K., Batonneau-Gener, I., Derriche, Z., Khelifa, A. (2011). Adsorptive properties of X zeolites modified by transition metal cation exchange. *Adsorption*, 17, 361–370. DOI: 10.1007/s10450-011-9336-4

[17] Khelifa, A., Hasnaoui, A., Derriche, Z., Bengueddach, A. (2001). Adsorption de CO_2 par des zéolithes X échangées par des cations bivalents. *Annales de Chimie Science des Matériaux*, 26, 55–66. DOI: 10.1016/S0151-9107(01)80046-5

[18] Halloui, C.L., Khelifa, M., Ziane, S., Marouf-Khelifa, K., Khelifa, A. (2025). Mechanistic understanding of the enhanced adsorption of diclofenac on a heat-treated and acid-leached halloysite. *International Journal of Environmental Analytical Chemistry*, 105(4), 727–745. DOI: 10.1080/03067319.2023.2270425

[19] Ziane, S., Marouf-Khelifa, K., Benmekki, H., Schott, J., Khelifa, A. (2015). Removal of a reactive textile azo dye by dolomitic solids: Kinetic, equilibrium, thermodynamic, and FTIR studies. *Desalination and Water Treatment*, 56, 695–708. DOI: 10.1080/19443994.2014.941308

[20] Boulett, A., Roa, K., Pizarro, G., Marambio, O., Santander, P., Sánchez, J. (2025). Polymeric resins with sulfonic or quaternary ammonium groups used as high-capacity adsorbents of tetracycline. *Reactive and Functional Polymers*, 217, 106487. DOI: 10.1016/j.reactfunctpolym.2025.106487

[21] Jung, S., Jung, M., Yoon, J., Kim, J., Jin, H.J., Kwak, H.W. (2024). Chitosan-derived activated carbon/chitosan composite beads for adsorptive removal of methylene blue and acid orange 7 dyes. *Reactive and Functional Polymers*, 204, 106028. DOI: 10.1016/j.reactfunctpolym.2024.106028

[22] Marouf-Khelifa, K., Khelifa, A., Belhakem, A., Marouf, R., Abdelmalek, F., Addou, A. (2004). The adsorption of pentachlorophenol from aqueous solutions onto exchanged Al-MCM-41 materials. *Adsorption Science & Technology*, 22(1), 1–12. DOI: 10.1260/026361704323150953

[23] Dhila, H., Bhapkar, A., Bhame, S. (2025). Metal oxide/biochar hybrid nanocomposites for adsorption and photocatalytic degradation of textile dye effluents: A review. *Desalination and Water Treatment*, 321, 101004. DOI: 10.1016/j.dwt.2025.101004

[24] Mehdi, K., Bendenia, S., Lecomte-Nana, G.L., Batonneau, I., Fabrice, G., Marouf-Khelifa, K., Khelifa, A. (2019). A new approach about the intercalation of hexadecyltrimethylammonium into halloysite: Preparation, characterization, and mechanism. *Chemical Papers*, 73, 131–139. DOI: 10.1007/s11696-018-0558-8

[25] Mahrez, N., Bessaha, F., Marouf-Khelifa, K., Çoruh, A., Khelifa, A. (2020). Performance and mechanism of interaction of crystal violet with organohalloysite. *Desalination and Water Treatment*, 207, 410–419. DOI: 10.5004/dwt.2020.26447

[26] Bao, J., Zhang, J., Tian, Y., Xu, H., Zheng, L., Bai, L., Liu, Y. (2024). Improving humidity sensor performance through phenylphosphonic acid-intercalated layered double hydroxide. *Materials Science in Semiconductor Processing*, 183, 108753. DOI: 10.1016/j.mssp.2024.108753

[27] Manoratne, C.H., Rajapakse, R.M.G., Dissanayake, M.A.K.L. (2006). Ionic conductivity of poly (ethylene oxide) (PEO)-montmorillonite (MMT) nanocomposites prepared by intercalation from aqueous medium. *International Journal of Electrochemical Science*, 1, 32–46. DOI: 10.1016/S1452-3981(23)17133-1

[28] Bessaha, F., Bessaha, G., Benhouria, A., Benalioua, B., Bendahma, F., Boucif, F., Mahrez, N., Ziane, S., Çoruh, A., Khelifa, A. (2024). Highly efficient batch adsorption of anionic dye in wastewater using nanocomposite: Experimental and theoretical studies. *Desalination and Water Treatment*, 317, 100292. DOI: 10.1016/j.dwt.2024.100292

[29] Mahmoudkhani, A.H., Langer, V. (2002). Phenylphosphonic acid as a building block for two-dimensional hydrogen-bonded supramolecular arrays. *Journal of Molecular Structure*, 609(1–3), 97–108. DOI: 10.1016/S0022-2860(01)00954-1

[30] Theng, B.K.G. (2024). The Chemistry of Clay-Organic Reactions (2nd ed.). Boca Raton: CRC Press. DOI: 10.1201/9781003080244

[31] Oloyede, O.G., Aroke, U.O., Giwa, S.O., Jock, A.A. (2021). Characterisation of natural and HDTMA-Br modified Dijah-Monkin bentonite clay: FTIR, XRF, XRD and SEM. *Path of Science*, 7(5), 2010–2018. DOI: 10.22178/pos.70-12

[32] Bessaha, F., Bessaha, G., Ziane, S., Khelifa, A. (2023). Adsorption of methyl orange on bentonite: Design, modeling, and analysis of experiments. *Iranian Journal of Chemistry and Chemical Engineering*, 42(10). DOI: 10.30492/ijcce.2023.1971110.5663

[33] Anirudhan, T.S., Ramachandran, M. (2015). Adsorptive removal of basic dyes from aqueous solutions by surfactant modified bentonite clay (organoclay): Kinetic and competitive adsorption isotherm. *Process Safety and Environmental Protection*, 95, 215–225. DOI: 10.1016/j.psep.2015.03.003

[34] Fernández, R., Vigil de la Villa, R., Ruiz, A.I., García, R., Cuevas, J. (2013). Precipitation of chlorite-like structures during OPC porewater diffusion through compacted bentonite at 90 °C. *Applied Clay Science*, 83–84, 357–367. DOI: 10.1016/j.clay.2013.07.021

[35] Cojocaru, C., Clima, L. (2020). Polymer assisted ultrafiltration of AO7 anionic dye from aqueous solutions: Experimental design, multivariate optimization, and molecular docking insights. *Journal of Membrane Science*, 604, 118054. DOI: 10.1016/j.memsci.2020.118054

[36] Bousemat, H., Ziane, S., Bessaha, F. (2025). Sustainable remediation of an anionic dye in aqueous solutions using modified aluminosilicate as a highly efficient and reusable adsorbent. *Reaction Kinetics, Mechanisms and Catalysis*, 138, 1517–1534. DOI: 10.1007/s11144-025-02794-3

[37] Bessaha, F., Mahrez, N., Bendenia, S., Kasmi, F., Marouf-Khelifa, K., Khelifa, A. (2017). Characterization and spectroscopic study of a heat-treated and acid-leached halloysite used in Congo Red adsorption. *International Journal of Intelligent Engineering and Systems*, 10(3), 272–279. DOI: 10.22266/ijies2017.0630.31

[38] Khalfa, A., Mellouk, S., Marouf-Khelifa, K., Khelifa, A. (2018). Removal of catechol from water by modified dolomite: Performance, spectroscopy, and mechanism. *Water Science and Technology*, 77, 1920–1930. DOI: 10.2166/wst.2018.071

[39] Bessaha, G., Bessaha, F., Bendenia, S., Khelifa, A. (2025). Exchanged zeolite adsorbent for removing Cr(VI): Kinetics, thermodynamics and adsorption mechanism. *International Journal of Environmental Analytical Chemistry*, 105(1), 1–19. DOI: 10.1080/03067319.2021.2006193

[40] Lagergren, S. (1898). Zur theorie der sogenannten adsorption geloster stoffe. *Kungliga Svenska Vetenskapsakademiens Handlingar*, 24(4), 1–39.

[41] Ho, Y.S., McKay, G. (1999). Pseudo-second order model for sorption processes. *Process Biochemistry*, 34(5), 451–465. DOI: 10.1016/S0032-9592(98)00112-5

[42] Weber, W.J., Morris, J.C. (1963). Kinetics of adsorption on carbon from solution. *Journal of the Sanitary Engineering Division, American Society of Civil Engineers*, 89, 31–59. DOI: 10.1061/JSEDAI.0000430

[43] Aharoni, C., Tompkins, F.C. (1970). Kinetics of adsorption and desorption and the Elovich equation. *In Advances in Catalysis* (Vol. 21, pp. 1–49). Academic Press. DOI: 10.1016/S0360-0564(08)60563-5

[44] Amar, A., Khelifa, M., Batonneau-Gener, I., Lecomte-Nana, G.L., Marouf-Khelifa, K., Çoruh, A., Khelifa, A. (2024). Improved ciprofloxacin removal by a novel organohalloysite obtained by phenylphosphonic acid intercalation. *Journal of Environmental Chemical Engineering*, 12, 111791. DOI: 10.1016/j.jece.2023.111791

[45] Yılmazoglu, M., Turan, B., Demircivi, P., Hızal, J. (2022). Synthesis and characterization of imidazolium based ionic liquid modified montmorillonite for the adsorption of Orange II dye: Effect of chain length. *Journal of Molecular Structure*, 1249, 131628. DOI: 10.1016/j.molstruc.2021.131628

[46] Shin, W.S. (2008). Competitive sorption of anionic and cationic dyes onto cetylpyridinium-modified montmorillonite. *Journal of Environmental Science and Health, Part A*, 43(12), 1459–1470. DOI: 10.1080/10934520802232337

[47] Bae, J.-H., Song, D.-I., Jeon, Y.-W. (2000). Adsorption of anionic dye and surfactant from water onto organomontmorillonite. *Separation Science and Technology*, 35(3), 353–365. DOI: 10.1081/SS-100100161

[48] Sarkar, B., Xi, Y., Megharaj, M., Naidu, R. (2011). Orange II adsorption on palygorskites modified with alkyl trimethylammonium and dialkyl dimethylammonium bromide—An isothermal and kinetic study. *Applied Clay Science*, 51(3), 370–374. DOI: 10.1016/j.clay.2010.11.032

[49] Yu, J., He, W., Liu, B. (2020). Adsorption of Acid Orange II with two-step modified sepiolite: Optimization, adsorption performance, kinetics, thermodynamics and regeneration. *International Journal of Environmental Research and Public Health*, 17, 1732. DOI: 10.3390/ijerph17051732

[50] Langmuir, I. (1918). The adsorption of gases on plane surfaces of glass, mica and platinum. *Journal of the American Chemical Society*, 40, 1361–1403. DOI: 10.1021/ja02242a004

[51] Freundlich, H. (1906). Over the adsorption in solution. *Zeitschrift für Physikalische Chemie*, 57, 385–470. DOI: 10.1515/zpch-1907-5723

[52] Jaroniec, M., Deryło, A., Marczewski, A.W. (1983). The Langmuir–Freundlich equation in adsorption from dilute solutions on solids. *Monatshefte für Chemie*, 114, 393–397. DOI: 10.1007/BF00798437

[53] Jaycock, M.J., Parfitt, G.D. (1981). *Chemistry of Interfaces*. Ellis Horwood Ltd. DOI: 10.1002/bbpc.19810850925

[54] Mahmoodian, H., Moradi, O., Tyagi, I., Maity, A., Asif, M., Gupta, V.K. (2015). Enhanced removal of methyl orange from aqueous solutions by poly(HEMA-chitosan-MWCNT) nanocomposite. *Journal of Molecular Liquids*, 202, 189–198. DOI: 10.1016/j.molliq.2014.10.040

[55] Xu, Y., Yu, X., Xu, B., Peng, D., Guo, X. (2021). Sorption of pharmaceuticals and personal care products on soil and soil components: Influencing factors and mechanisms. *Science of the Total Environment*, 753, 141891. DOI: 10.1016/j.scitotenv.2020.141891

[56] Leone, V.O., Pereira, M.C., Aquino, S.F., Oliveira, L.C.A., Correa, S., Ramalho, T.C., Gurgel, L.V.A., Silva, A.C. (2018). Adsorption of diclofenac on a magnetic adsorbent based on maghemite: Experimental and theoretical studies. *New Journal of Chemistry*, 42, 437–449. DOI: 10.1039/C7NJ03214E

[57] Xing, X., Qu, H., Shao, R., Wang, Q., Xie, H. (2017). Mechanism and kinetics of dye desorption from dye-loaded carbon (XC-72) with alcohol-water system as desorbent. *Water Science and Technology*, 76(5), 1243–1250. DOI: 10.2166/wst.2017.268

[58] Chern, J.M., Wu, C.Y. (2001). Desorption of dye from activated carbon beds: Effects of temperature, pH, and alcohol. *Water Research*, 35, 4159–4165. DOI: 10.1016/S0043-1354(01)00127-0

[59] Bagotia, N. (2025). Regeneration strategies for exhausted adsorbents used in water treatment — a critical review. *Journal of Water Process Engineering*, 69, 106560. DOI: 10.1016/j.jwpe.2024.106560

[60] Bessaha, F., Bessaha, G., Benhouria, A., Benalioua, B., Mahrez, N., Boucif, F., Ziane, S., Bendahma, F., Çoruh, A., Khelifa, A. (2025). Efficient removal of a pharmaceutical compound on organoclay: Batch experiment, DFT calculation, statistical physics, and modelling. *Chemical Engineering Communications*, 212, 695–712. DOI: 10.1080/00986445.2024.2428964

[61] Breen, C., D'Mello, N., Yarwood, J. (2002). The thermal stability of mixed phenylphosphonic acid/water intercalates of kaolin and halloysite: A TG–EGA and VT-DRIFTS study. *Journal of Materials Chemistry*, 12, 273–278. DOI: 10.1039/B104254H

[62] Bao, J., Zhang, J., Tian, Y., Xu, H., Bai, L.Z.L., Liu, Y. (2024). Improving humidity sensor performance through phenylphosphonic acid-intercalated layered double hydroxide. *Materials Science in Semiconductor Processing*, 183, 108753. DOI: 10.1016/j.mssp.2024.108753

[63] Gentile, M.B., Gomez, S.R., Avena, M.J., Luengo, C.V. (2025). The interaction of phenylphosphonic acid with the surface of goethite: Isotherms, kinetics, electrophoretic mobility and ATR-FTIR spectroscopy. *Environmental Pollution*, 371, 125938. DOI: 10.1016/j.envpol.2025.125938

[64] Kgabi, D.P., Ambushe, A.A. (2023). Characterization of South African bentonite and kaolin clays. *Sustainability*, 15, 12679. DOI: 10.3390/su151712679

[65] Bauer, C., Jacques, P., Kalt, A. (1999). Investigation of the interaction between a sulfonated azo dye AO7 and a TiO_2 surface. *Chemical Physics Letters*, 307, 397–406. DOI: 10.1016/S0009-2614(99)00518-7

[66] Abbott, L.C., Batchelor, S.N., Oakes, J., Gilbert, B.C., Whitwood, A.C., Lindsay Smith, J.R., Moore, J.N. (2005). Experimental and computational studies of structure and bonding in parent and reduced forms of the azo dye Orange II. *The Journal of Physical Chemistry A*, 109 (14), 2894–2905. DOI: 10.1021/jp045216s

[67] Trchová, M., Šeděnková, I., Konyushenko, E.N., Stejskal, J., Holler, P., Ćirić-Marjanović, G. (2006). Evolution of polyaniline nanotubes: The oxidation of aniline in water. *The Journal of Physical Chemistry B*, 110(19), 9461–9468. DOI: 10.1021/jp057528g

[68] Drohat, A.C., Stivers, J.T. (2000). Escherichia coli uracil DNA glycosylase: NMR characterization of the short hydrogen bond from His187 to uracil O2. *Biochemistry*, 39(38), 11865–11875. DOI: 10.1021/bi000922e

[69] Khezami, L., Ben Aissa, M. A., Modwi, A., Guesmi, A., Algethami, F.K., Bououdina, M. (2024). Efficient removal of organic dyes by Cr-doped ZnO nanoparticles. *Biomass Conversion and Biorefinery*, 14, 4177–4190. DOI: 10.1007/s13399-022-02952-w

[70] Hoehn, R.D., Carignano, M.A., Kais, S., Zhu, C., Zhong, J., Zeng, X.C., Francisco, J.S., Gladich, I. (2016). Hydrogen bonding and orientation effects on the accommodation of methylamine at the air–water interface. *The Journal of Chemical Physics*, 144(21), 214701. DOI: 10.1063/1.4950951

[71] Kim, D.-S. (2003). Measurement of point of zero charge of bentonite by solubilization technique and its dependence of surface potential on pH. *Environmental Engineering Research*, 8(4), 222–227. DOI: 10.4491/eer.2003.8.4.222

[72] Phillips, B.L., Mason, H.E., Guggenheim, S. (2007). Hydrogen bonded silanols in the 10 Å phase: Evidence from NMR spectroscopy. *American Mineralogist*, 92(8–9), 1474–1485. DOI: 10.2138/am.2007.2417

[73] Jayne, B.N. (2005). Hydrogen-bonded layer structures based on guanidinium sulfonates (*Doctoral Dissertation*, University of Bath, United Kingdom). University of Bath Repository.

[74] Koo, M.-J., Lee, S.-H., Yun, H., Kim, J. W., Rotermund, F., Kwon, O.-P. (2015). New electro-optic N-methylquinolinium crystals with naphthalene-1-sulfonate. *Bulletin of the Korean Chemical Society*, 36(12), 2920–2923. DOI: 10.1002/bkcs.10568

[75] Jing, L., Li, P., Li, Z., Ma, D., Hu, J. (2025). Influence of π–π interactions on organic photocatalytic materials and their performance. *Chemical Society Reviews*, 54, 2054–2090. DOI: 10.1039/D4CS00029C

[76] Yang, Y., Adhikari, S., Xu, G. (2021). Molecular dynamics simulation in the interlayer of mixed-layer clays due to hydration and swelling mechanism. *Crystals*, 11(6), 586. DOI: 10.3390/cryst11060586.